Article

Not peer-reviewed version

A DFT Investigation of SF_6 Decomposition Products Adsorption on V-doped Graphene/MoS_2 Heterostructures

Aijuan Zhang *, Xinwei Chang , Tingting Liu , Jiayi An , Xin Liu , Yike Cui , Keqi Li , Xianrui Dong

Posted Date: 25 February 2026

doi: 10.20944/preprints202602.1284.v1

Keywords: SF_6; adsorption properties; Graphene/MoS_2 heterostructure; DFT

 doi:10.20944/preprints202602.1284.v1

Article

A DFT Investigation of SF_6 Decomposition Products Adsorption on V-doped Graphene/ MoS_2 Heterostructures

Aijuan Zhang *, Xinwei Chang, Tingting Liu, Jiayi An, Xin Liu, Yike Cui, Keqi Li and Xianrui Dong

College of Physica and Electronics Engineering, Xianyang Normal University, Shannxi Province, China; zhangaj@xync.edu.cn

* Correspondence: zhangaj@xync.edu.cn

Abstract

The detection of SF_6 decomposition products is essential for diagnosing insulation faults in gas-insulated switchgear. Using first-principles density functional theory, this study investigates the adsorption behavior of five characteristic gases (H_2S, SO_2, SOF_2, SO_2F_2, and SF_6) on pristine and vanadium-doped graphene/MoS_2 (GMV) heterostructures to evaluate their potential for gas sensing applications. Pristine graphene/MoS_2 exhibits weak physisorption toward all target molecules, with low adsorption energies and negligible charge transfer, indicating insufficient sensitivity for practical use. To address this limitation, a V-doped graphene/MoS_2 heterostructure is proposed, wherein vanadium atoms are incorporated into the graphene lattice to introduce active centers and modulate interfacial charge transfer. The results demonstrate that H_2S, SO_2, and SOF_2 preferentially adsorb atop the V site via local covalent interactions, with significantly enhanced adsorption energies (up to −0.388 eV for SO_2) and shortened distances. In contrast, SO_2F_2 and SF_6 adsorb near electron-depleted carbon regions driven by electrostatic attraction. Charge density difference and Bader charge analyses reveal pronounced charge redistribution upon SO_2 and SF_6 adsorption, while density of states analysis confirms orbital hybridization near the Fermi level, suggesting possible chemical bond formation. Notably, adsorption of SO_2 and SF_6 substantially reduces the density of states at near Fermi level, indicating a measurable modulation of surface conductivity. These findings establish V-doped graphene/MoS_2 as a promising sensing material for selective detection of SF_6 decomposition products, offering a viable strategy for advancing online monitoring technologies in power systems.

Keywords: SF_6; adsorption properties; Graphene/MoS2 heterostructure; DFT

1. Introduction

Sulfur hexafluoride (SF_6), the primary insulating medium used in Gas-insulated switchgear (GIS), exhibits exceptional chemical stability, arc-quenching capability, and resistance to decomposition [1]. Nevertheless, insulation defects—such as metallic protrusions, loose contacts leading to floating potentials, insulation aging, and chemical corrosion—may arise during manufacturing, transportation, installation, and maintenance [2–6]. These defects distort the internal electric field and trigger partial discharge, arcing, or localized overheating, which subsequently induce decomposition of SF_6 into low-fluorine sulfides (e.g., SF_4, SF_3) [7]. These unstable intermediates undergo irreversible reactions with trace impurities (e.g., H_2O, O_2) in the gas atmosphere, forming stable byproducts including H_2S, SO_2, SOF_2, and SO_2F_2 [8]. The accumulation of such decomposition products not only reduces the SF_6 concentration but also generates acidic compounds upon hydrolysis (e.g., SO_2, H_2S), which corrode metallic components and solid insulation materials. These processes collectively degrade the dielectric performance of GIS and may precipitate severe insulation failures, posing significant risks to the secure and stable operation of power grids.

 doi:10.20944/preprints202602.1284.v1

Accumulating evidence suggests that the composition and concentration of SF_6 decomposition products are closely correlated with specific types of insulation defects, offering a viable pathway for condition assessment of GIS [8]. In engineering practice, however, the decomposition products are typically present at trace levels and involve multiple gas species, rendering their accurate detection technically challenging. Gas sensor technology, which relies on gas-sensitive materials that transduce adsorption-induced changes in electrochemical properties into measurable electrical signals (e.g., resistance variation), has emerged as a promising approach for quantitative and qualitative analysis of SF_6 byproducts [9,10]. This method enables rapid detection, miniaturized instrumentation, and compatibility with automated online monitoring systems. Nonetheless, conventional gas sensors suffer from inherent limitations including poor selectivity toward single gas components, pronounced cross-sensitivity, and insufficient long-term stability. Moreover, the complex and uncommon nature of SF_6 decomposition products necessitates the development of gas sensors specifically tailored to these characteristic species.

Nanomaterial-based gas sensors have garnered considerable research interest owing to their ultracompact dimensions and low power consumption [11–16]. Heterostructures composed of graphene and molybdenum disulfide (MoS_2) have demonstrated enhanced sensitivity toward target gas molecules through interfacial charge transfer modulation [17–22]. Despite these advances, no systematic investigation has been reported to date on the gas-sensing performance of graphene/MoS_2 heterostructures toward SF_6 and its typical decomposition products.

In this work, we systematically explore the adsorption properties of graphene/MoS_2 heterostructures toward SF_6 and its primary decomposition gases (SO_2, H_2S, SOF_2, and SO_2F_2) using density functional theory (DFT) calculations. Our results indicate that pristine graphene exhibits weak adsorption and poor selectivity toward these molecules, while sole modulation of the MoS_2 component or structure fails to concurrently achieve optimized sensing responses for multiple target gases. To overcome these limitations, we propose—for the first time—the precise incorporation of vanadium (V) atoms into the graphene lattice, a strategy distinct from conventional doping of the MoS_2 layer or random heterointerface modification. This design confers dual functionality upon the vanadium dopants: they serve as active centers that modulate interfacial charge transfer to amplify electrical signal variations induced by gas adsorption, and simultaneously act as specific recognition sites that substantially enhance the selective adsorption of sulfur- and oxygen-containing decomposition products. Importantly, this approach preserves the intrinsic high-conductivity network of graphene while establishing synergistic coupling with the semiconducting properties of MoS_2. Collectively, these features enable the directional tuning and systematic optimization of the overall gas-sensing performance of the heterostructure, offering a promising pathway for advanced SF_6 decomposition product detection.

2. Materials and Methods

In this paper, we explored the geometric optimization, charge distribution, density of states (DOS), and other related properties of Graphene/Mos_2 heterostructure with five kinds of gas molecule (SF_6, H_2S, SO_2, SOF_2, SO_2F_2) based on first-principles, using the DFT in the Vienna Ab initio Simulation Package (VASP) software, which is based on the plane-wave pseudopotential method. The electron exchange and correlation were described by the Perdew-Burke-Ernzerhof (PBE) function of the generalized gradient approximation (GGA) based on density functional theory (DFT). The core electron and valence electron were treated using the Projected Augmented Wave method (PAW). Van der Waals (vdW) interactions were corrected for using the Grimme's DFT-D3 method [23–26]. The cutoff energy was set as 500 eV. The Monkhorst-Pack k-grid was chosen as 4 × 4 × 1. We set vacuum about 15 Å to avoid the interaction from adjacent unit. For the system energy calculation, The energy tolerance accuracy, maximum force, and displacement were set as 1×10^{-5} Ha, 2×10^{-3} Ha/Å and 5×10^{-3} Å [27–33]. The Bader charge analysis method is utilized to determine the charge transfer and distribution within the system. All calculations incorporate spin polarization. The adsorption energy (E_{ads}) is defined as equation (1):

 doi:10.20944/preprints202602.1284.v1

$$E_{ads}=E_{gas/sub}-E_{sub}-E_{gas} \quad (1)$$

Where $E_{gas/sub}$, E_{sub} and E_{gas} represent the total energy of the whole adsorption system, the energy of adsorption substrate and the energy of isolated gas molecules before the adsorption, respectively. According to this formula, the larger the absolute value of the adsorption energy calculated, the greater the energy difference before and after the adsorption process. Generally, this indicates a stronger adsorption effect.

The charge density difference (Δρ) is calculated as Equation (2):

$$\Delta\rho=\rho_{gas/sub}-\rho_{sub}-\rho_{gas} \quad (2)$$

Where $\rho_{gas/sub}$ is the total charge density of the whole adsorption system, ρ_{sub} and ρ_{gas} are the charge density of adsorption substrate and isolated one gas molecule, respectively.

Based on Mulliken charge analysis, the charge transfer (Q_T) between gas molecules and adsorption substrate was calculated by following equation:

$$Q_T = Q_{ads} - Q_{iso} \quad (3)$$

Where Q_{ads} and Q_{iso} are total charges of molecule before and after adsorption, respectively.

3. Results and Discussion

3.1. Adsorbing Characteristics of G/MoS_2 Interface for Target Gases

To obtain the adsorption characteristics of G/MoS_2 to the SF_6 decomposition gas products, the structures of G/MoS_2 and gas molecules were initially optimized. The G/MoS_2 was established based on the 3×3 × 1 supercell structure of monolayer MoS_2 and the 4 × 4 × 1 supercell structure of graphene with lattice mismatch about 2%, as shown in Figure 1. The Mo-S bond length is 2.42 Å and that of C-C is 1.41 Å. The optimized distance between MoS_2 interlayer and graphene interlayer is 3.42 Å, which is in good accordance with experimentally research [34] and this distance demonstrate that vdW force exists in this heterostructure.

The models of SF_6 and the four typical decomposition gases (H_2S, SO_2, SOF_2, SO_2F_2) were optimized, as shown in Figure 2. It is can be observed from Figure 2 (e) that there are six F atoms are symmetrical around a S atom in the form of regular octahedral structure in the SF_6 molecule. The bond angels of F-S-F are 90.55° and the bond lengths of F-S are 1.60 Å. The H_2S molecule appears a high symmetrical "V" shape with an angel of 91.76° between two S-H bonds and a length of 1.35 Å S-H bond, as shown in Figure 2 (a). The shape of SO_2 and H_2S seem to be like, but it shows in Figure 2 (b) that the angel of two O-S bonds is 120.12° and the length of O-S bond is 1.46 Å. The SOF_2 molecule present tetrahedral structure and symmetrical about the O-S bond. The angel between the O-S bond and F-S bond is 106.55°, the length of O-S bond is 1.43 Å and that of the F-S bond is 1.64 Å. As shown in Figure 2 (d), SO_2F_2 is symmetric with respect to the perpendicular bisector of the line connecting either the two O atoms or the two F atoms. The bond angels of O-S-F, O-S-O and F-S-F are 108.28°, 124.98° and 95.72°, respectively. The bond lengths of O-S and F-S are 1.42 Å and 1.57 Å, respectively. We have confirmed that these calculations give very close results to published data [35].

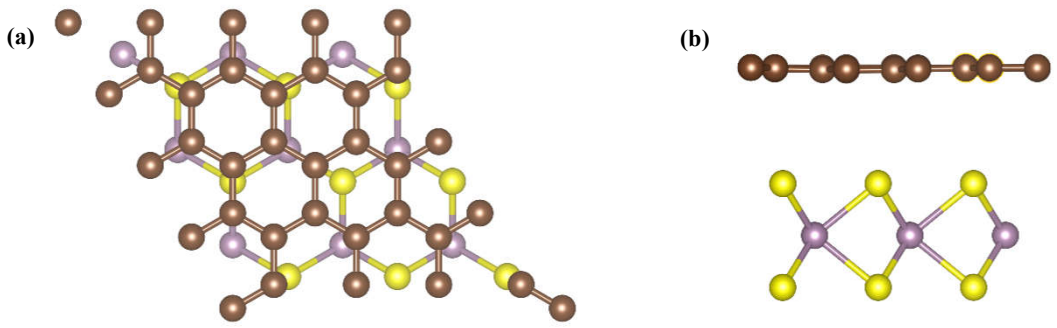

Figure 1. Geometric structure of optimized G/MoS_2 heterostructure, (a) vertical view (b) side view.

 doi:10.20944/preprints202602.1284.v1

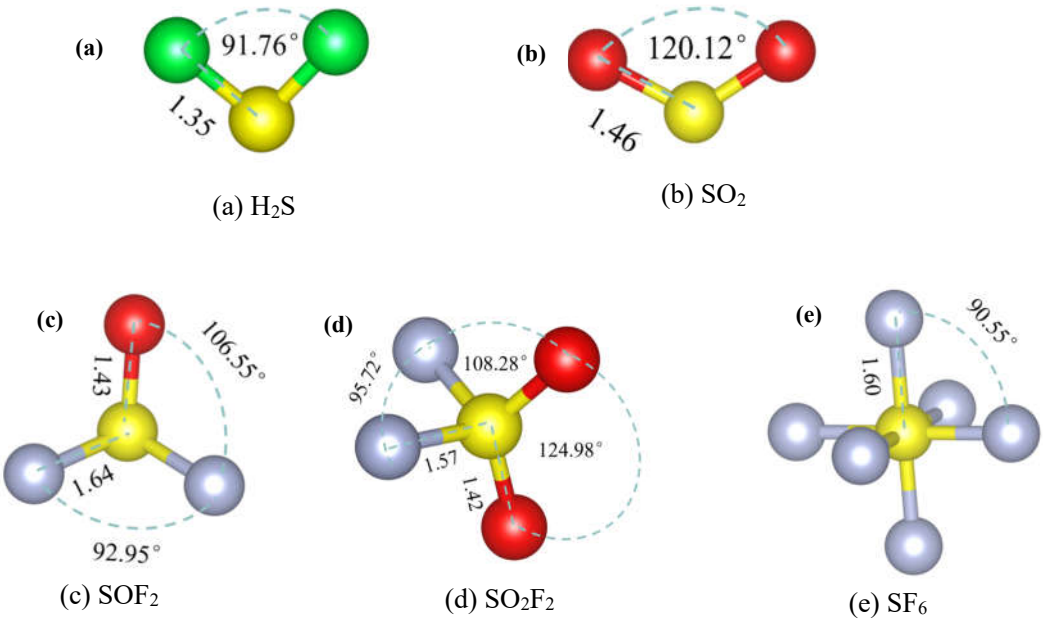

(a) H_2S (b) SO_2 (c) SOF_2 (d) SO_2F_2 (e) SF_6

Figure 2. Optimized molecular structure of H_2S, SO_2, SOF_2, SO_2F_2 and SF_6.

The adsorption models were obtained by position the SF_6 and other four decomposition gas molecules close to the surface of the optimized G/MoS_2 heterostructure model and the initial distances are about 3 Å. The structure of these adsorption systems were optimized, with the K-point selected as 3×3×1 grids at the Gamma point. After these structure optimization, static calculations were conducted. These accurate adsorption energies were ultimately obtained from the static calculations. On those basis, other calculations were carried out to obtain more parameters characterizing the adsorption properties. In this paper, parameters such as density of states and charge difference density were selected for calculation. The paper considered the different adsorption positions and directions of each gas at the G/MoS_2 interface, and selected the most stable adsorption structure from the calculation results for analysis. After structural optimization and static calculation, the adsorption energies and minimum distances corresponding to the adsorption models of each gas molecule and G/MoS_2 were obtained and are shown in Table 1. In Table 1, the minimum distance is the shortest distance between the atoms of the adsorbed gas molecule and the surface atoms of G/MoS_2. Figure 3 presents the stable adsorption configurations of five gas molecules on G/MoS_2.

Table 1. Adsorption energy, distance and charge transfer between SF_6 decomposition gas and G/MoS_2 heterostructure.

Species	E_{ad}/eV	D /Å	ΔQ/e
G/MoS_2-H_2S	-0.196	2.96	-0.01
G/MoS_2-SO_2	-0.181	3.32	-0.05
G/MoS_2-SOF_2	-0.141	2.97	-0.01
G/MoS_2-SO_2F_2	-0.164	2.97	0.02
G/MoS_2-SF_6	-0.241	2.92	-0.02

 doi:10.20944/preprints202602.1284.v1

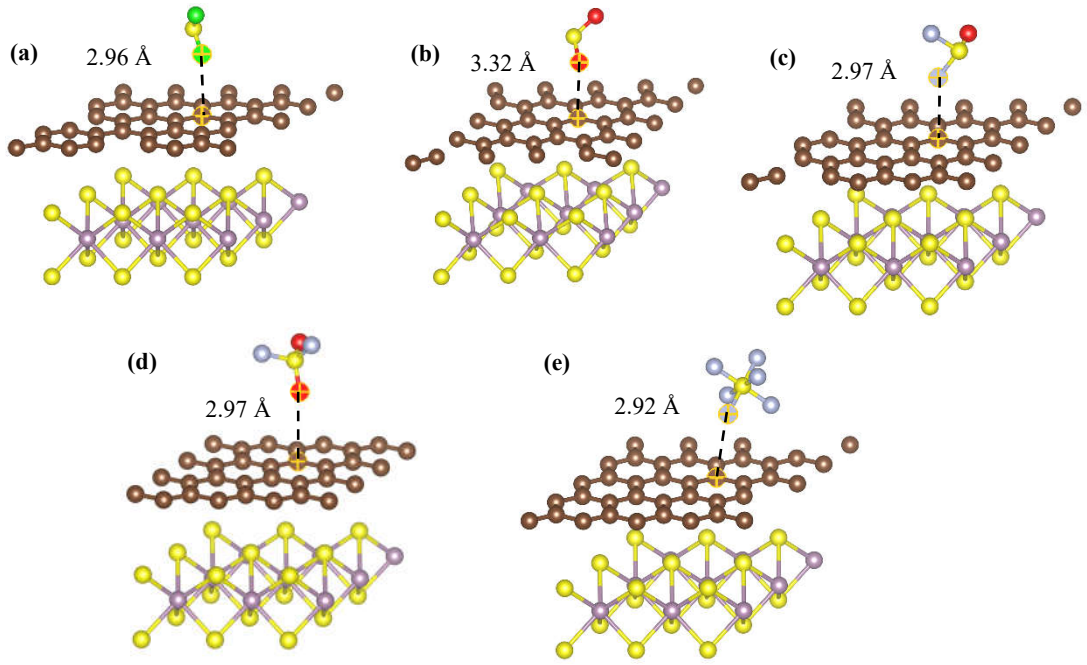

Figure 3. Adsorption structure of G/MoS_2 interface for H_2S, SO_2, SOF_2, SO_2F_2 and SF_6.

The corresponding adsorption parameters, including adsorption distance (*D*), adsorption energy E_{ad}, and charge transfer Q_T, are summarized in Table 1. A positive charge transfer value indicates that electrons are transferred from gas molecules to the adsorption substrate, while a negative value indicates that electrons are transferred from the adsorption substrate to the gas molecules. By comparing the adsorption energies, the distances and charge transfer value between the five gas molecules and G/MoS_2, it is found that the adsorption between the five gas molecules and G/MoS_2 in this calculation is all relatively weak physical adsorption. Therefore, while the intrinsic graphene/MoS_2 heterostructure offers a fundamental platform for gas adsorption, its limited adsorption strength, weak charge transfer, and insufficient selectivity toward SF_6 decomposition products render it inadequate for reliable gas-sensing applications. To overcome these intrinsic bottlenecks, heteroatom doping—particularly with transition metals—has emerged as an effective strategy to modulate the local electronic structure, enhance chemical reactivity, and introduce gas-specific recognition sites.

3.2. Adsorbing Characteristics of V-Doped G/MoS_2 (GMV) for Target Gases

In this section, we focus on V-doped graphene/MoS_2 heterostructures. Vanadium is selected due to its unfilled d orbitals, moderate electronegativity, and proven catalytic activity in sulfur-containing gas interactions. We first establish the stable configurations of V-doped graphene and its heterostructure with MoS_2, followed by a systematic analysis of the adsorption behavior, charge transfer, and electronic response toward SO_2, H_2S, SOF_2, and SO_2F_2.

Figure 4(a) top view showing the atomic-scale structure of the V-doped graphene layer. The doping site (V_1) and its surrounding carbon atoms (C_1–C_{31}) within the graphene lattice are explicitly labeled. The vanadium atom forms covalent bonds with three adjacent carbon atoms, exhibiting bond lengths of approximately 1.88 Å for V_1–C_{21} and V_1–C_{26}, and 1.96 Å for V_1–C_{25}. These bond lengths are significantly larger than the intrinsic C–C bond length in pristine graphene (1.41 Å), indicating pronounced local lattice distortion induced by V doping. This configuration corresponds to the lowest-energy stable doping site, with all atomic positions fully relaxed via density functional theory calculations. Figure 5(b) side view illustrating the layered stacking relationship of the V-doped graphene/MoS_2 heterostructure. The bottom layer comprises monolayer MoS_2, where S and Mo atoms adopt a trigonal prismatic coordination. The top layer consists of V-doped monolayer graphene, in which a vanadium atom substitutes a carbon atom and is incorporated into the graphene lattice. The

 doi:10.20944/preprints202602.1284.v1

optimized interlayer distance is approximately 3.58 Å, suggesting the formation of a stable heterojunction governed by van der Waals interactions. The vertical distance between the V atom and the graphene layer is approximately 1.52 Å, while that between the V atom and the MoS_2 layer is approximately 2.06 Å. Bader charge analysis indicates that approximately 0.398 e is transferred from the V atom to the MoS_2 layer. Concurrently, about 0.933 e is transferred to the graphene layer, with the majority (approximately 0.831 e) accumulated on the C_{21}, C_{25}, and C_{26} atoms.

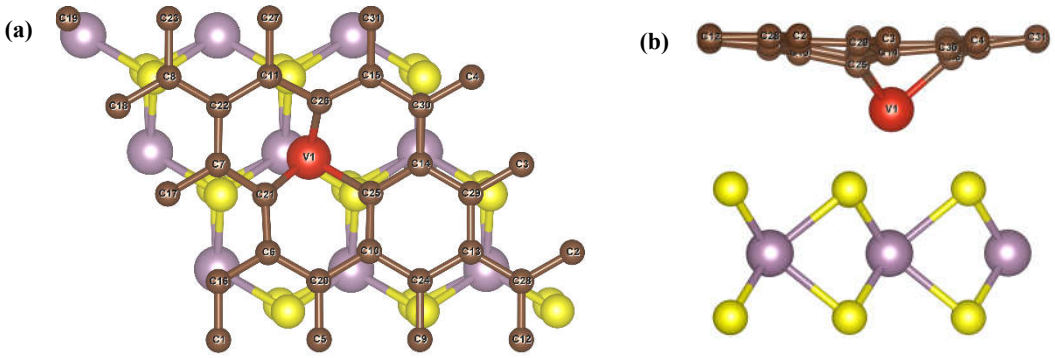

Figure 4. Optimized geometric configurations of the V-doped graphene/MoS_2 heterostructure. (a) top view, (b) side view.

Figure 5 presents the optimized geometric configurations of H_2S, SO_2, SOF_2, SO_2F_2, and SF_6 adsorbed on the V-doped graphene/MoS_2 heterostructure surface, all of which were obtained via density functional theory (DFT) calculations with full atomic relaxation to the lowest-energy states. Analysis of the top and side views reveals that H_2S, SO_2, and SOF_2 molecules preferentially adsorb in the vicinity of the V doping site, confirming that the vanadium atom serves as an active center that substantially enhances the heterostructure's affinity toward sulfur-containing decomposition products. In contrast, SO_2F_2 and SF_6 molecules tend to adsorb near the positively charged carbon atoms (C_{18}, C_{22}, C_{23}, and C_{27}) induced by charge transfer, this behavior is attributed to the sulfur atoms in SO_2F_2 and SF_6 being surrounded by highly electronegative oxygen or fluorine atoms, rendering them locally electron-deficient and thereby facilitating electrostatic attraction with the electron-depleted carbon sites. Specifically, the H_2S molecule is stably adsorbed with its sulfur atom oriented toward the vanadium atom and its two hydrogen atoms pointing toward the graphene surface, resulting in a slight tilt of the molecular plane relative to the substrate, and an adsorption height of approximately 2.03 Å. The SO_2 molecule adopts an orientation nearly parallel to the graphene surface, with an adsorption height of 2.34 Å. The SOF_2 molecule anchors via its sulfur atom atop the vanadium dopant, exhibiting an inverted tetrahedral configuration and positioned approximately 2.18 Å above the graphene layer. For SO_2F_2, two fluorine atoms and one oxygen atom are located above the electron-depleted carbon atoms C_{22}, C_{23}, and C_{27}, respectively, corresponding to an adsorption height of about 3.02 Å. The SF_6 molecule is arranged such that three fluorine atoms point toward C_{18}, C_{22}, and C_{23}, respectively, with the entire molecule situated approximately 2.85 Å above the graphene layer. The adsorption heights of the five gas molecules follow the order: SO_2F_2 > SF_6 > SO_2 > SOF_2 > H_2S. Compared with the pristine (undoped) graphene/MoS_2 heterostructure, the adsorption distances for all gas molecules except SO_2F_2 are significantly reduced, with the most pronounced decreases observed for H_2S, SO_2, and SOF_2. These results demonstrate that V doping not only introduces specific recognition sites for gas molecules but also effectively tailors the adsorption behavior via modulation of the surface charge distribution, thereby establishing a robust structural foundation for subsequent analyses of charge transfer mechanisms and gas-sensing response performance.

 doi:10.20944/preprints202602.1284.v1

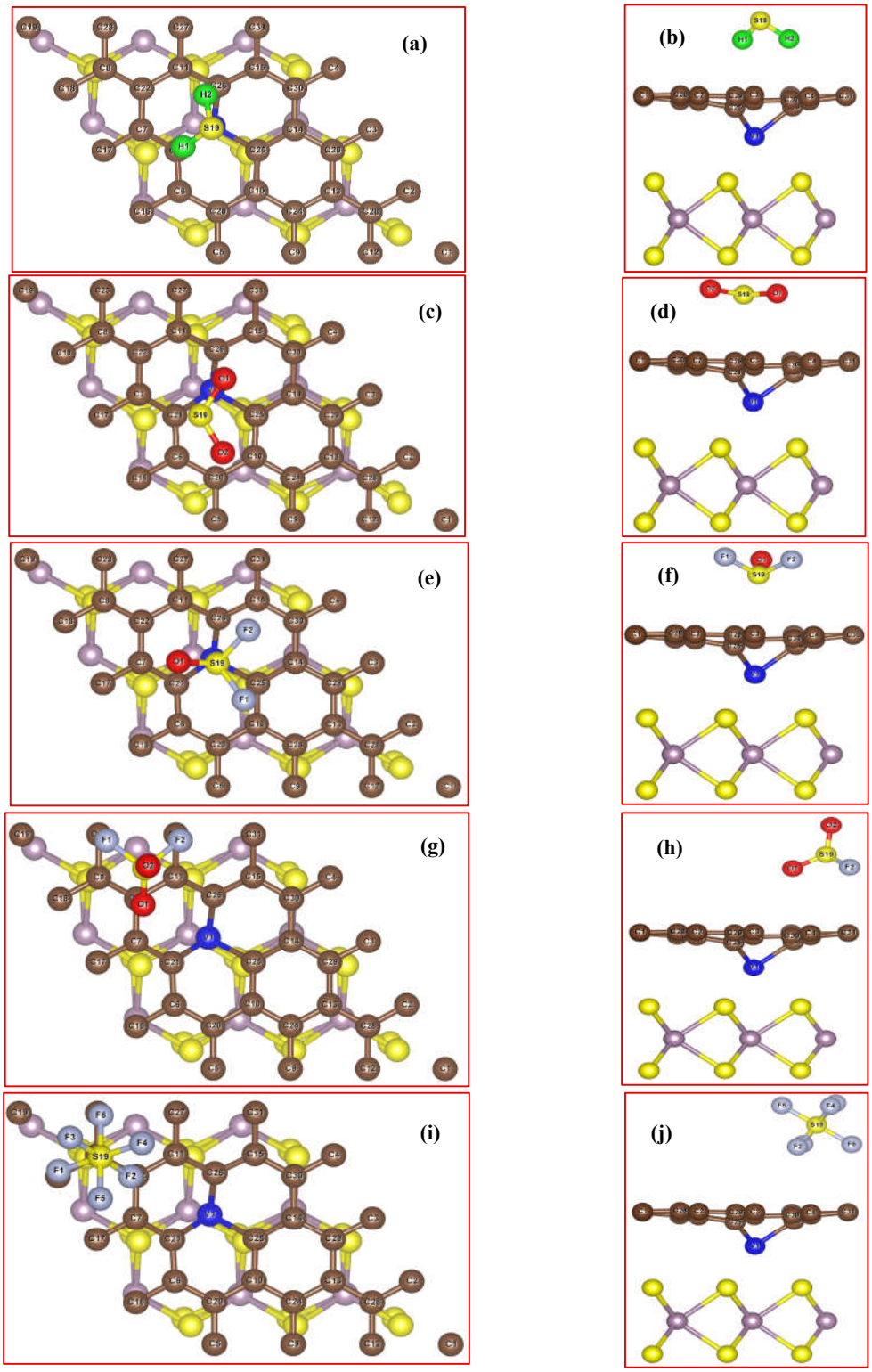

Figure 5. Optimized geometric configurations for the adsorption of five characteristic SF_6 decomposition products on the V-doped graphene/MoS_2 heterostructure: (a, b) H_2S, (c, d) SO_2, (e, f) SOF_2, (g, h) SO_2F_2, and (i, j) SF_6. Top views are shown in (a), (c), (e), (g), and (i), while the corresponding side views are presented in (b), (d), (f), (h), and (j).

Table 2 summarizes the adsorption energy, adsorption distance (D), and Bader charge transfer (ΔQ) for five characteristic SF_6 decomposition products adsorbed on the V-doped graphene/MoS_2 heterostructure (GMV) surface. The calculated results reveal two distinct adsorption regimes depending on the molecular species. H_2S, SO_2 and SOF_2 preferentially adsorb atop the vanadium dopant site via local covalent bonding, forming stable configurations with relatively short adsorption

 doi:10.20944/preprints202602.1284.v1

distances (2.03 Å, 2.34 Å and 2.18 Å, respectively). In contrast, SO_2F_2, and SF_6 tend to adsorb in the vicinity of positively charged carbon atoms (e.g., C_{18}, C_{22}, C_{23}, C_{27}) induced by charge redistribution, with the adsorption driving force primarily originating from electrostatic attraction and van der Waals interactions, accompanied by adsorption distances of 3.03 Å, and 2.85 Å, respectively. Notably, all five gas molecules exhibit adsorption energies within a moderate range (-0.224 to -0.380 eV), indicating physisorption or weak chemisorption.

Table 2. Adsorption energy, distance and charge transfer between SF6 decomposition gas and V-doped G/MoS2 heterostructure.

Species	E_{ad}/eV	D /Å	ΔQ/e
GMV-H_2S	-0.241	2.03	0.01
GMV-SO_2	-0.380	2.34	-0.06
GMV-SOF_2	-0.317	2.18	-0.027
GMV-SO_2F_2	-0.268	3.03	-0.017
GMV-SF_6	-0.224	2.85	-0.021

Based on charge density files computed using the VASP, further analyses were conducted with the assistance of the vaspkit code to generate the charge density difference plots for the V-doped MoS_2 system before and after the adsorption of H_2S, SO_2, SOF_2, SO_2F_2, and SF_6 gas molecules, as depicted in Figure 6. Using the Z-axis lattice parameter of the GMV supercell as a reference, the ordinate in Figure 6 represents the distance along this direction. The plane-averaged charge density difference plots (Figures 6(a), 6(c), 6(e), 6(g), and 6(i)) reveal significant charge redistribution at the interface between GMV and all adsorbed gas molecules except H_2S, suggesting a strong interaction between these molecules and the GMV substrate. This is further corroborated by the three-dimensional isosurface plots (Figures 6(b), 6(d), 6(f), 6(h), and 6(j)), where purple and cyan regions denote electron accumulation and depletion, respectively.

Notably, substantial electron accumulation is observed around the adsorbed gas molecules. A particularly pronounced electron accumulation is evident on the GMV surface following SO_2F_2 adsorption, which may indicate a like-charge repulsion effect, potentially limiting its adsorption capability. Collectively, these charge transfer characteristics are consistent with the trends in adsorption energy and adsorption configurations reported earlier.

By comparing the total density of states (TDOS) of the GMV system after gas adsorption with the projected density of states (PDOS) of the adsorbed gas molecules, the influence of the adsorbed gas molecules on the electronic properties of the adsorption system can be elucidated. A comparison of the density of states for GMV adsorbed with H_2S, SO_2, SOF_2, SO_2F_2, and SF_6 molecules is presented in Figure 7, where the Fermi level is indicated by a dashed line. Figure 7(c) and (f) present the total density of states (TDOS) of the GMV system after SO_2 and SF_6 adsorption, along with the projected density of states (PDOS) of the corresponding gas molecules. The analysis reveals that the PDOS of the 2p orbitals of these gas molecules exhibit pronounced peaks near the Fermi level, which hybridize or interact with the TDOS of the adsorption system, suggesting the possible formation of chemical bonds between the gas molecules and the substrate. This observation indicates strong adsorption of SO_2 and SF_6 on GMV, consistent with the previously discussed adsorption energies, geometric configurations, and charge density difference analyses. In contrast, as illustrated in Figure 7(b), the PDOS of H_2S, SOF_2 and SO_2F_2 have a negligible impact on the electronic structure of GMV near the Fermi level, implying weak adsorption of these gases on GMV, which aligns with the aforementioned findings. Furthermore, compared to the TDOS of pristine GMV, a significant reduction in the density of states near the Fermi level is observed upon SO_2 and SF_6 adsorption, indicating that gas adsorption modulates the electronic structure of the substrate, potentially influencing its surface conductivity.

 doi:10.20944/preprints202602.1284.v1

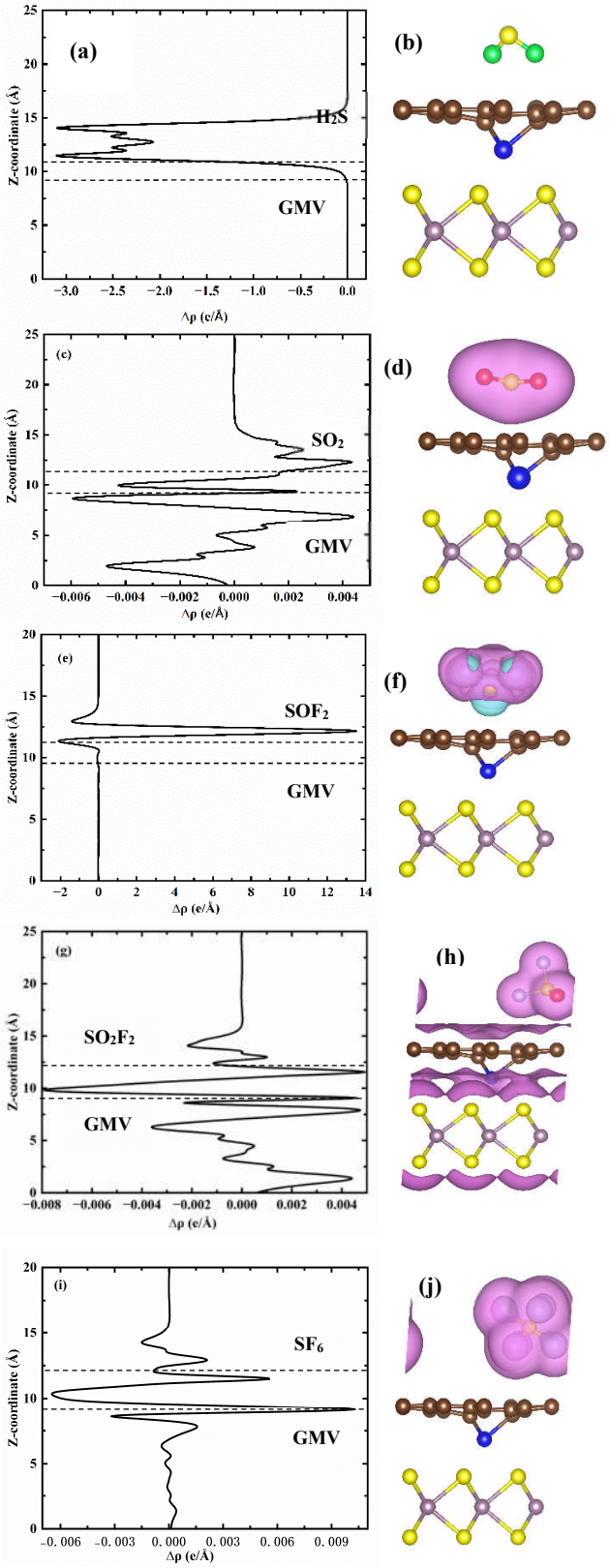

Figure 6. Plane-averaged differential charge density (DCD) for (a) H_2S, (c) SO_2, (e) SOF_2, (g) SO_2F_2 and (i) SF_6 adsorbed on Co-doped G/MoS_2 (GMV) surface. The (b), (d), (f), (h) and (i) show the top views of 0.006 e$Å^{-3}$ DCD isosurfaces.

 doi:10.20944/preprints202602.1284.v1

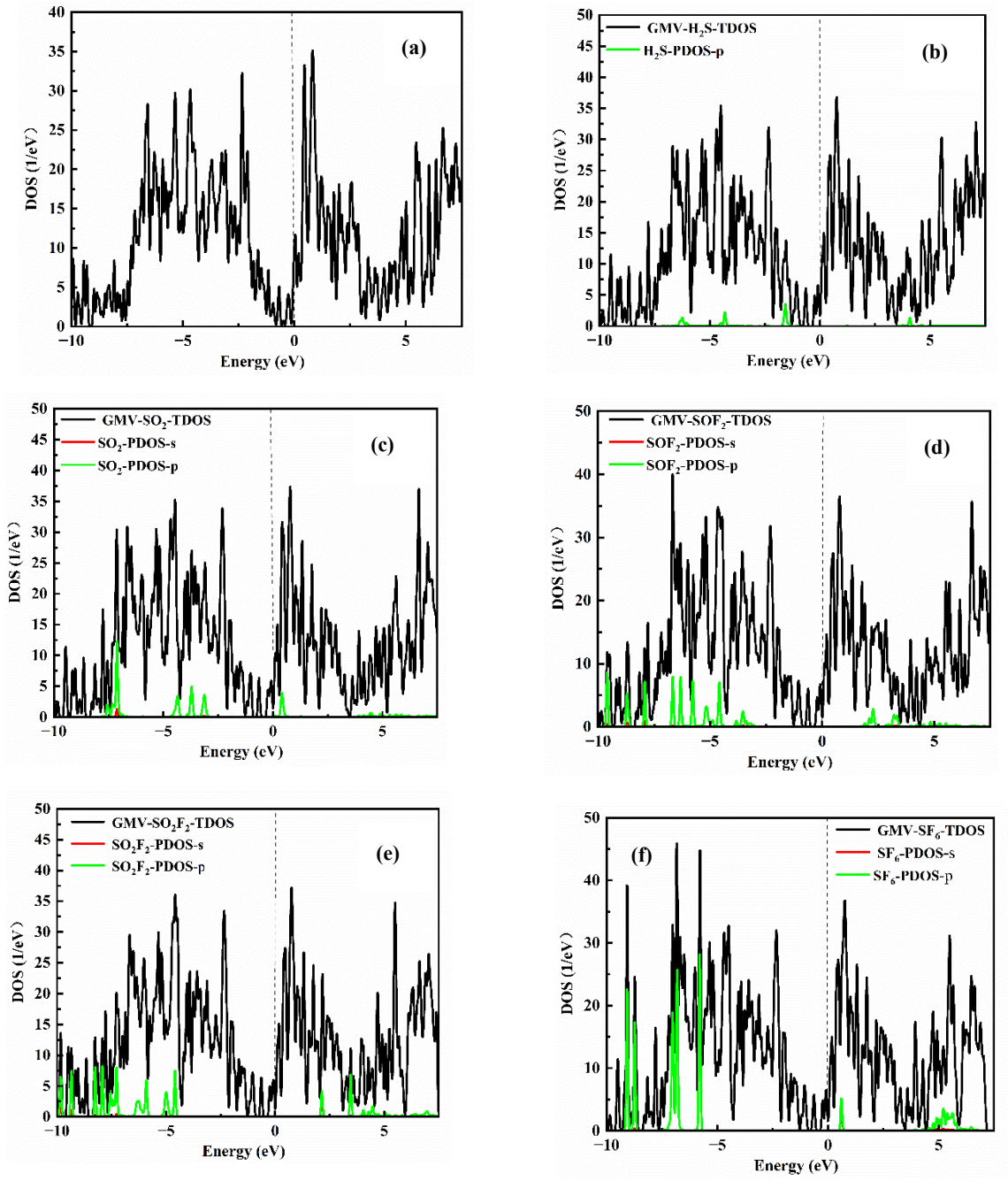

Figure 7. The TDOS of the GMV and GMV surface with H_2S, SO_2, SOF_2, SO_2F_2, SF_6 gas molecules, and the PDOS of the adsorbed gas molecules.

4. Conclusions

Herein, the adsorption behavior and electronic properties of five characteristic SF_6 decomposition gases, namely H_2S, SO_2, SOF_2, SO_2F_2, and SF_6, on pristine and vanadium-doped graphene/MoS_2 heterostructures are systematically investigated via first-principles density functional theory (DFT). Computational results reveal that the pristine graphene/MoS_2 heterostructure exhibits weak physical adsorption toward all the aforementioned gas molecules, characterized by low adsorption energies and minimal charge transfer, which are insufficient to meet the sensitivity and selectivity requirements for gas-sensing applications. By incorporating vanadium atoms into the graphene lattice to construct V-doped graphene/MoS_2 heterostructures, their adsorption performance is significantly enhanced. The introduction of V atoms forms localized active centers within the graphene layer, effectively modulating the interfacial charge distribution. It is

 doi:10.20944/preprints202602.1284.v1

found that H_2S, SO_2, and SOF_2 molecules preferentially adsorb at the top sites of V atoms through localized covalent interactions, with markedly increased adsorption energies (reaching -0.388 eV for SO_2) and shortened adsorption distances. Notably, the adsorption of SO_2 and SF_6 is accompanied by significant interfacial charge redistribution and orbital hybridization, indicating strong interactions between these molecules and the substrate. In contrast, SO_2F_2 and SF_6 are primarily adsorbed at the electron-deficient carbon regions induced by V doping, with electrostatic interactions dominating the adsorption driving force. Density of states (DOS) analysis further confirms that the 2p orbitals of SO_2 and SF_6 hybridize with the substrate's DOS near the Fermi level, leading to a substantial reduction in the DOS at the Fermi level, which implies detectable changes in surface conductivity. In conclusion, the V-doped graphene/MoS_2 heterostructure demonstrates differentiated adsorption responses and enhanced electronic coupling characteristics toward SF_6 decomposition gases, particularly exhibiting promising sensitivity potential in the detection of SO_2 and SF_6. This study provides a theoretical foundation for the design of novel gas sensors for SF_6 decomposition products and the realization of online monitoring of GIS insulation status.

Author Contributions: Conceptualization, A. Z., J. A, X. L., Y. C., K. L., and X. D.; methodology, T. L.; software, A. Z.; validation, X.C.; formal analysis, A. Z.; investigation, A. Z.; resources, A. Z.; data curation, A. Z.; writing—original draft preparation, A. Z.; writing—review and editing, A. Z.; visualization, A. Z.; supervision, A. Z.; project administration, A. Z.; funding acquisition, A. Z, Tingting. L., X. C. All authors have read and agreed to the published version of the manuscript.

Funding: This research was funded by the National Natural Science Foundation of China (NSFC), grant number 12304092, the Natural Science Basic Research Plan in Shaanxi Province of China, grant number 2023-JC-YB-032, the 2025 Basic and Vocational Education Practical Research Project of Xianyang Normal University, grant number sjxm202574, the Natural Science Basic Research Program of Shaanxi Province, grant number 2025JC-YBQN-097, Chongqing New Youth Innovation Talent Program, grant number CSTB2024NSCQ-QCXMX0086, National-level Undergraduate Innovation Training Program, grant number 202510722028; The Natural Science Basic Research Program of Shaanxi Province, grant number 2024JC-YBQN-0020; the Scientific Research Program of Shaanxi Province Education Department, grant number 24JK0702.

Data Availability Statement: Not applicable.

Acknowledgments: We would like to thank all the co-authors for their contributions to this work.

Conflicts of Interest: The authors declare that they have no known competing financial interests or personal relationships that could have appeared to influence the work reported in this paper.

References

1. Khan, B. *et al.* Analysis of the dielectric properties of R410A Gas as an alternative to SF_6 for high-voltage applications. *High Voltage* **4**, 41–48 (2019).
2. Tsai, W.-T. The decomposition products of sulfur hexafluoride (SF6): Reviews of environmental and health risk analysis. *Journal of Fluorine Chemistry* **128**, 1345–1352 (2007).
3. Malik, N. & Qureshi, A. A Review of Electrical Breakdown in Mixtures of SF6 and Other Gases. *IEEE Trans. Elect. Insul.* **EI-14**, 1–13 (1979).
4. Xiao, S., Zhang, X., Tang, J. & Liu, S. A review on SF 6 substitute gases and research status of CF 3 I gases. *Energy Reports* **4**, 486–496 (2018).
5. Vanbrunt, R. J. Production rates for oxyfluorides SOF2, SO2F2, and SOF4 in SF6 corona discharges. *J. RES. NATL. BUR. STAN.* **90**, 229 (1985).
6. Dervos, C. T. & Vassiliou, P. Sulfur Hexafluoride (SF_6): Global Environmental Effects and Toxic Byproduct Formation. *Journal of the Air & Waste Management Association* **50**, 137–141 (2000).
7. Dibeler, V. H. & Mohler, F. L. Dissociation of SF6, CF4, and SiF4 by electron impact. *J. RES. NATL. BUR. STAN.* **40**, 25 (1948).

 doi:10.20944/preprints202602.1284.v1

8. Zhong, L. *et al.* Theoretical study of the chemical decomposition mechanism and model of Sulfur hexafluorid (SF6) under corona discharge. *Journal of Fluorine Chemistry* **220**, 61–68 (2019).
9. Luo, C. *et al.* Transition Metal (Co, V, W, Zr) Single-Atom Decorated Biphenylene for Enhancing the Sensing Performance of SF_6 Decomposition Molecules. *Langmuir* **40**, 9490–9500 (2024).
10. Zeng, F., Li, H., Cheng, H., Tang, J. & Liu, Y. SF_6 decomposition and insulation condition monitoring of GIE: A review. *High Voltage* **6**, 955–966 (2021).
11. Zhang, W., Gui, Y., Yang, Y. & Tang, C. A hybrid nanogenerator based on wind energy harvesting for powering self-driven sensing systems. *Journal of Cleaner Production* **429**, 139550 (2023).
12. Shao, Y. *et al.* Core-sheath structured CNT@Ni-CNT fiber-based multifunctional fabric with high-sensitivity, wide-range strain sensing, and enhanced electromagnetic shielding absorption. *Chemical Engineering Journal* **512**, 162358 (2025).
13. Wang, Y., Gui, Y., He, S. & Yang, J. Hybrid nanogenerator driven self-powered SO2F2 sensing system based on TiO2/Ni/C composites at room temperature. *Sensors and Actuators B: Chemical* **377**, 133053 (2023).
14. Gui, Y., Wang, Y., He, S. & Yang, J. Self-powered smart agriculture real-time sensing device based on hybrid wind energy harvesting triboelectric-electromagnetic nanogenerator. *Energy Conversion and Management* **269**, 116098 (2022).
15. Chen, Y. *et al.* Integrated design and optimization of magnetically actuated self-sensing flexible gripper with fast response, high stability, and high payload-to-weight ratio. *Sci. China Technol. Sci.* **68**, 1920206 (2025).
16. He, S., Gui, Y., Wang, Y. & Yang, J. A self-powered β-Ni(OH)2/MXene based ethanol sensor driven by an enhanced triboelectric nanogenerator based on β-Ni(OH)2@PVDF at room temperature. *Nano Energy* **107**, 108132 (2023).
17. Ma, H. *et al.* Humidity sensing characteristics of graphene and MoS2 as well as their heterostructures with different stacking configurations.
18. Cho, B. *et al.* Chemical Sensing of 2D Graphene/MoS_2 Heterostructure device. *ACS Appl. Mater. Interfaces* **7**, 16775–16780 (2015).
19. Ghayyem, F., Kiakojouri, A., Frank, I. & Nadimi, E. Gas Sensing Properties of Graphene/MoS_2/Graphene Lateral Heterostructure: A First Principles Investigation. *IEEE Sensors J.* **24**, 36334–36341 (2024).
20. Alzate-Carvajal, N. & Luican-Mayer, A. Functionalized Graphene Surfaces for Selective Gas Sensing. *ACS Omega* **5**, 21320–21329 (2020).
21. Bag, A. & Lee, N.-E. Gas sensing with heterostructures based on two-dimensional nanostructured materials: a review. *J. Mater. Chem. C* **7**, 13367–13383 (2019).
22. Baloglu, A. B. *et al.* GRAPHENE/BN VAN DER WAALS HETEROSTRUCTURES FOR ENHANCED TOXIC GAS SENSING.
23. Li, B., Zhang, N., Lei, Y., Zhu, M. & Yang, H. Graphene/Chalcogenide Heterojunctions for Enhanced Electric-Field-Sensitive Dielectric Performance: Combining DFT and Experimental Study. *Nanomaterials* **16**, 128 (2026).
24. Fang, Q. *et al.* van der Waals graphene/MoS_2 heterostructures: tuning the electronic properties and Schottky barrier by applying a biaxial strain. *Mater. Adv.* **3**, 624–631 (2022).
25. Foruzan, E., Akmal, A. A. S., Niayesh, K., Lin, J. & Sharma, D. D. Comparative study on various dielectric barriers and their effect on breakdown voltage. *High Voltage* **3**, 51–59 (2018).
26. Grimme, S., Antony, J., Ehrlich, S. & Krieg, H. A consistent and accurate *ab initio* parametrization of density functional dispersion correction (DFT-D) for the 94 elements H-Pu. *The Journal of Chemical Physics* **132**, 154104 (2010).
27. Hartmann, G., Lee, M. & Hwang, G. S. Structural, electronic and adsorption properties of monolayer 2H-MoS2 on graphene substrates: A computational study. *Inorganic Chemistry Communications* **106**, 135–138 (2019).
28. Wei, H., Gui, Y., Kang, J., Wang, W. & Tang, C. A DFT Study on the Adsorption of H2S and SO2 on Ni Doped MoS2 Monolayer. *Nanomaterials* **8**, 646 (2018).
29. Zou, Y. *et al.* Charge Transfer in Graphene-MoS_2 Vertical Heterostructures Tuned by Stacking Order and Substrate-Introduced Electric Field. *ACS Appl. Mater. Interfaces* **16**, 30589–30597 (2024).

 doi:10.20944/preprints202602.1284.v1

30. Cao, Q. *et al.* Controllable Graphene/MoS_2 Heterointerfaces by Perpendicular Surface Functionalization. *Angew Chem Int Ed* **63**, e202415922 (2024).
31. Miao, H. *et al.* DFT analysis of the sensitivity of graphene/MoS2 heterostructures toward H2CO. *Vacuum* **214**, 112182 (2023).
32. Zhang, W. *et al.* Effects of vertical strain and electrical field on electronic properties and Schottky contact of graphene/MoSe2 heterojunction. *Journal of Physics and Chemistry of Solids* **157**, 110189 (2021).
33. Liu, X. & Li, Z. Electric Field and Strain Effect on Graphene-MoS_2 Hybrid Structure: Ab Initio Calculations. *J. Phys. Chem. Lett.* **6**, 3269–3275 (2015).
34. Pierucci, D. *et al.* Band Alignment and Minigaps in Monolayer MoS_2 -Graphene van der Waals Heterostructures. *Nano Lett.* **16**, 4054–4061 (2016).
35. Li, B., Zhou, Q., Peng, R., Liao, Y. & Zeng, W. Adsorption of SF6 decomposition gases (H2S, SO2, SOF2 and SO2F2) on Sc-doped MoS2 surface: A DFT study. *Applied Surface Science* **549**, 149271 (2021).